Available online at www.sciencedirect.com
SCIENCE DIRECT
Tectonophysics 421 (2006) 231–250
TECTONOPHYSICS
www.elsevier.com/locate/tecto

Spatial variations in the similarity of earthquake populations: The case of the 1997 Colfiorito–Sellano (northern Apennines, Italy) seismic sequence

Mauro Alberti *

Museo Nazionale dell'Antartide, Via Laterina, 8, I - 53100 Siena, Italy

Received 2 December 2005; received in revised form 8 April 2006; accepted 26 April 2006
Available online 21 June 2006

This paper is dedicated to the memory of Prof. Francesco Antonio Decandia.

Abstract

The spatial properties of events in the 1997 Colfiorito–Sellano seismic sequence (Northern Apennines, Italy) were investigated using coherence, a parameter derived from seismic moment tensors that quantifies the kinematic similarity between focal mechanisms. The 1997 Colfiorito–Sellano seismic sequence predominantly consists of normal faulting earthquakes, with a few strike-slip and reverse faulting episodes. This kinematic heterogeneity is possibly related to the contemporaneous activity of two different sets of faults: NW–SE normal faults and NNE–SSW sub-vertical faults, the latter inherited from the previous Miocene compressional phase. The study used two independently-derived data sets of the same seismic sequence characterized by a different number of events and by different precision of spatial localisation. Their statistical significances, assessed through a reshuffling procedure, reveal that data sets with at least some hundreds of events and good positional precision are required to obtain significant results through coherence analysis. Results from the better quality data set indicate that this seismic sequence is characterized by a rapid decrease in the kinematic similarity between earthquake pairs within 2 km of separation, particularly along directions sub-perpendicular to the normal fault strike. The decrease rate seems to be controlled by the geometric characteristics of the normal faults, given that the mean along-dip distance between fault segments is 2 km. In proximity to pre-existing tectonic lineaments the relative abundance of strike-slip and reverse faults tends to decrease the kinematic similarity between events but does not influence the coherence decrease rate. The presence of mixed focal mechanisms (normal, reverse and strike-slip) in a single seismic phase implies that mixed fault types are not restricted to polyphase tectonic histories: such heterogeneous kinematics during a single phase may be induced by the presence of inherited discontinuities.

Keywords: Earthquake population; Spatial analysis; Coherence; 1997 Colfiorito–Sellano seismic sequence

1. Introduction

An earthquake can be considered as the equivalent of a single phase of fault activity, and seismic sequences as a temporal slice of a tectonic phase (e.g. Ramsay and Huber, 1987, p. 564). The quantitative spatio-temporal analysis of earthquake populations may thus provide an actualistic model of a tectonic phase, and can be compared to the observed characteristics of geological fault populations. In particular, statistically-based spatio-temporal analysis can highlight systematic variations in fault/earthquake characteristics, such as the kinematic similarity between focal mechanisms, which may in turn

* Fax: +39 0577 233890.
E-mail address: albertim@unisi.it.

0040-1951/$ - see front matter © 2006 Elsevier B.V. All rights reserved.
doi:10.1016/j.tecto.2006.04.015

be related to geological factors such as stress field variations, kinematic compatibilities (Marrett and Allmendinger, 1990), or post-kinematic folding processes. Direction of analysis and time lag between two observations may influence the value of examined variables. A lack of directional or temporal variations in kinematic similarity may indicate that the examined area is structurally homogeneous.

The 1997 Colfiorito–Sellano seismic sequence in the Northern Apennines is a seismologically and geologically well-characterized sequence (Amato et al., 1998; Ekström et al., 1998) and may thus be used for spatial analyses. This sequence developed over a few months time in an area of more than 500 km^2 currently undergoing extension (Lavecchia et al., 1994) or transtension (Cello et al., 1997). Focal mechanisms were mainly extensional, but strike-slip and reverse focal mechanisms were also observed (Cattaneo et al., 2000; Chiaraluce et al., 2004). The presence of strike-slip events has been ascribed to the reactivation of oblique lineaments inherited from the previous compressive tectonic phase, while reverse events show no clear spatial relationships with the other structures (Chiaraluce et al., 2003, 2005). This study applies the coherence parameter (Kagan and Knopoff, 1985a,b) to two independent data sets (Cattaneo et al., 2000; Chiaraluce et al., 2004) derived from this seismic sequence with the aim of investigating and comparing temporal and spatial variations in the kinematic similarity. Particular attention was devoted to the kinematic and dynamic role of Miocene reverse-dextral faults in the current extensional tectonic phase. These analyses may help to clarify the influence of complex and inherited tectonic structures on the spatial characteristics of subsequent tectonic phases.

2. Methodology for spatial analysis of fault/earthquake similarities

Spatial analysis of the geometric similarity between earthquakes and faults requires the use of quantitative methods for defining the similarity between faults, such as the coherence method (Kagan and Knopoff, 1985b; Kagan, 1992a), spherical-grid searches of compatible stress fields (Nemcok and Lisle, 1995), the right-dihedra method (Nemcok et al., 1999) or determining the minimum rotation angle required to make two focal mechanisms coincide (Kagan, 1990, 1991, 1992b). We adopt the coherence method of Kagan and Knopoff (1985a,b) and Kagan (1992a) due to its simple analytical form and to the availability of a GIS software for spatial analysis (Alberti, 2005). The method and the theoretical coherence distribution resulting from simulations of homogeneous and heterogeneous stress fields are explained in Alberti (2006) and will only be summarized here. Additional information is provided in the case of simulation results.

Coherence is calculated from the correlation tensor between two fault/earthquake normalized moment tensors (Kagan and Knopoff, 1985b). A normalized moment tensor D_{ij} is a symmetric, second-rank tensor with six

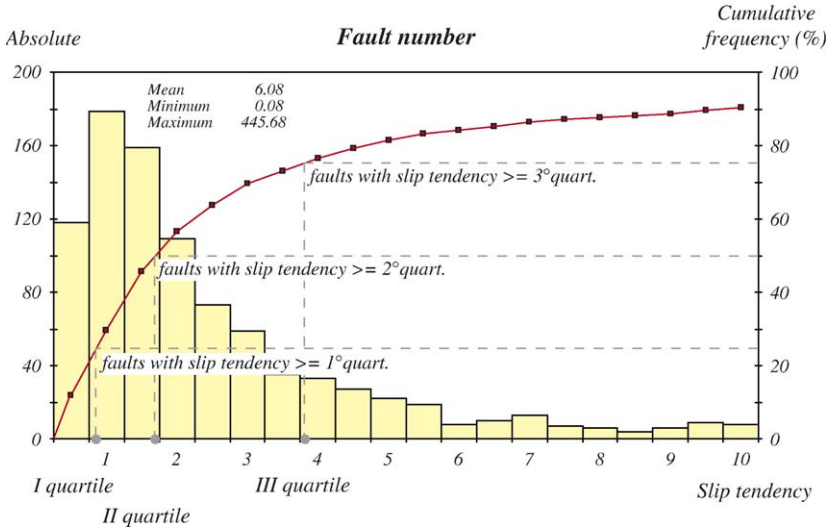

Fig. 1. Diagram of absolute (left) and cumulative (right) fault number vs. slip tendency value, as derived by a simulation considering 1000 randomly oriented surfaces subject to a homogeneous stress field with a stress ratio of 0.5 (data from Alberti, 2006). The cumulative curve allows the definition of slip tendency quartiles (fault percentages of 25%, 50% and 75%).

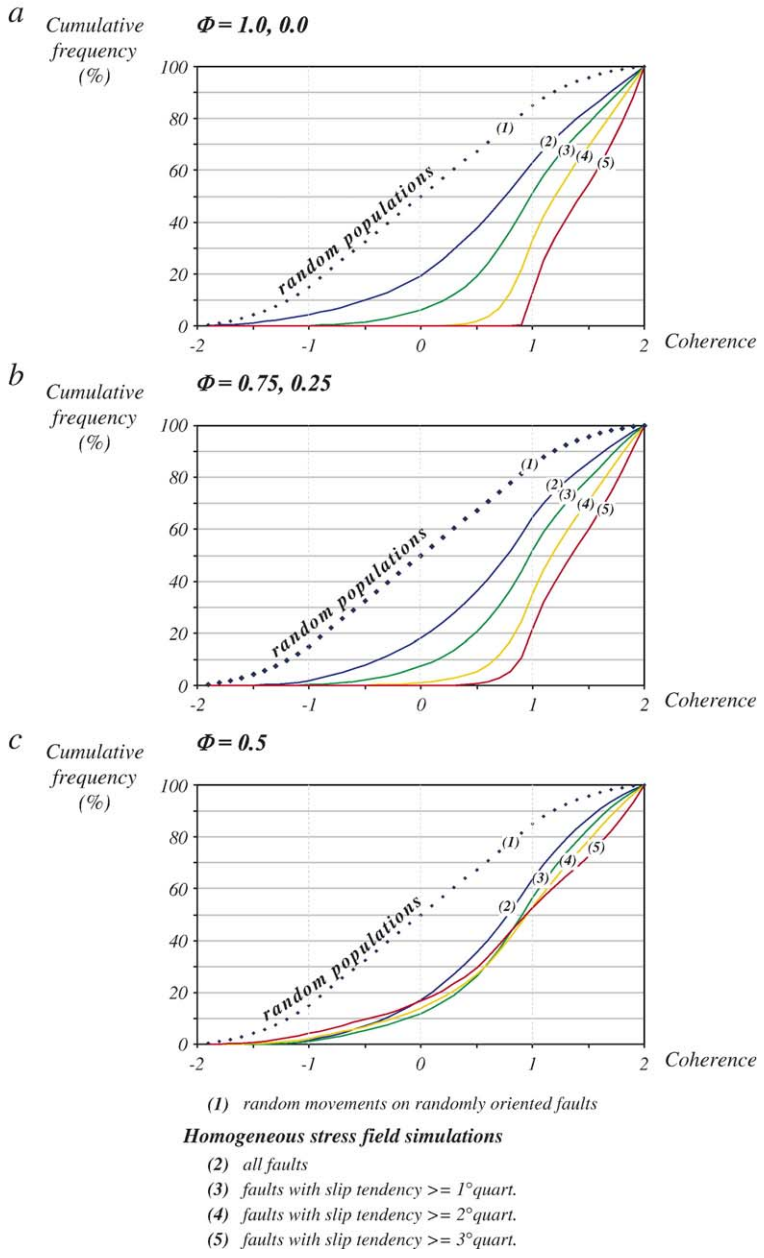

Fig. 2. Cumulative coherence distributions resulting from random and homogeneous stress field simulations: (a) stress ratios Φ=1.0 and 0.0, (b) Φ=0.75 and 0.25, (c) Φ=0.5. Results are divided according to different distributions with increasing slip tendency values (cf. Fig. 1).

independent components (due to its symmetry), expressed as:

$$d_{ij} = 0.5(\mathbf{u}_i\boldsymbol{\nu}_j + \mathbf{u}_j\boldsymbol{\nu}_j) \quad (i,j = 1,2,3) \tag{1}$$

where $\boldsymbol{u}$ (with Cartesian components u_1, u_2, u_3) is the slip vector and $\boldsymbol{\nu}$ (ν_1, ν_2, ν_3) is the vector normal to the fault plane. Given its symmetric nature, the tensor is the same irrespective of which of the two planes is actually the fault plane and which is the nodal plane: this method is thus applicable to both faults and earthquakes.

The correlation tensor is symmetric and of fourth-order, characterized by a set of invariants whose number depends on the isotropy of the medium and the seismic tensor characteristics: one of these invariants, J_3, is independent of location and time:

$$J_3 = < m_{ij}n_{ij} > \tag{2}$$

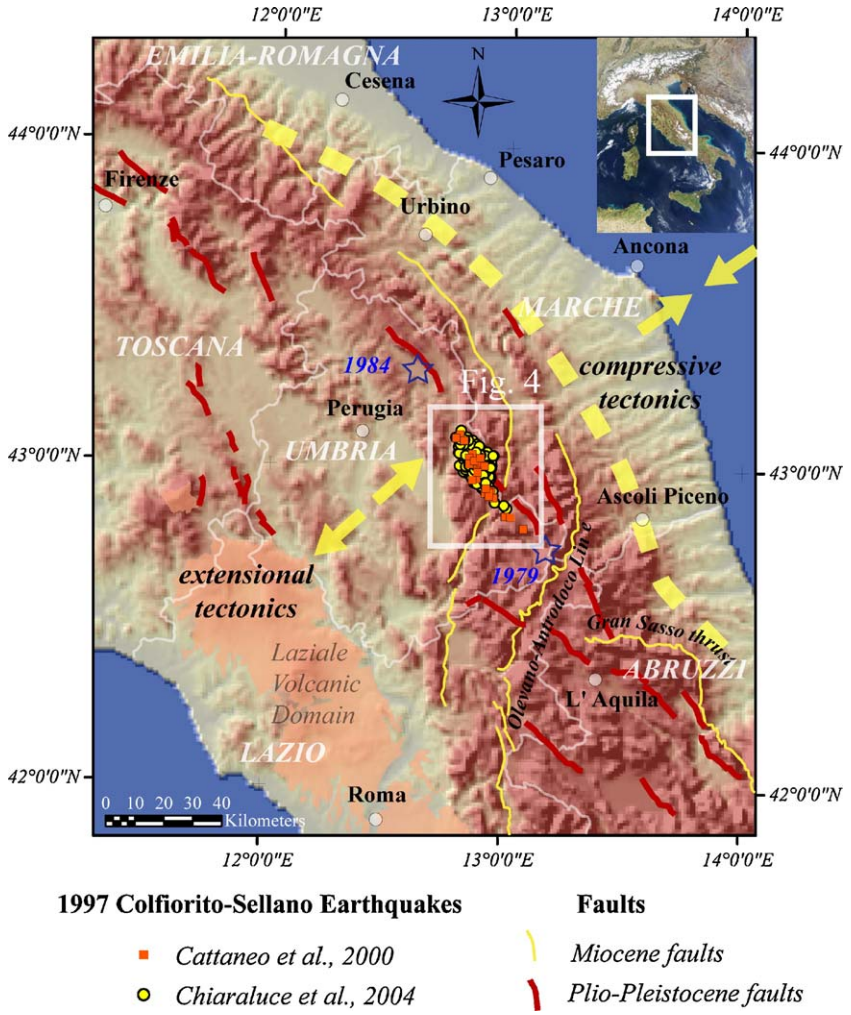

Fig. 3. Structural sketch map of the northern Apennines (Italy), with major tectonic lineaments and locations of the 1997 Colfiorito–Sellano earthquake data sets (from Cattaneo et al., 2000; Chiaraluce et al., 2004), along with the epicentres of 1979 Norcia and 1984 Perugia earthquakes (stars). The dashed line indicates the approximate boundary between areas undergoing extension after the compressive phase (to the west) and those still undergoing compression (to the east) (modified after Lavecchia et al., 1994, Fig. 11).

where the brackets indicate the average value, and m_{ij} and n_{ij} are the components of the two considered seismic tensors.

The ratio J_3/I_2 (where I_2 is a constant value), named coherence by Kagan and Knopoff (1985b), ranges from 2.0 to −2.0: the maximum value is obtained for two equal tensors, the minimum one for two opposite tensors. The adopted terminology for the similarity between fault/earthquake pairs is based on that of Kagan and Knopoff (1985b): a pair is termed coherent if its coherence is between 2 and 1, incoherent if its coherence is between −1 and 1, and anti-coherent if its coherence is less than −1.

The resulting distribution of coherence values can be considered a statistical summary of the structural similarity of the analyzed fault/earthquake data set, which can be compared with distributions derived from simulations of surfaces with random movements or with movements induced by a uniform or variable stress field under the Bott (1959) assumption (i.e. slip parallel to the resolved shear stress on a plane).

Different values of the stress ratio Φ (Orife and Lisle, 2003 and references therein):

$$\Phi = \frac{\sigma_2 - \sigma_3}{\sigma_1 - \sigma_3} \tag{3}$$

(the Φ range is between 0, for $\sigma_2 = \sigma_3$, and 1, for $\sigma_1 = \sigma_2$) and of the statistical distribution of *slip tendency* s_t values (sensu Morris et al., 1996):

$$s_t = \tau/\sigma_N \tag{4}$$

(τ is the shear stress while σ_N is the normal stress acting on a surface) were used to assess their influence on the resulting coherence distributions.

Using a simulated data set of 1000 uniformly-distributed surfaces, theoretical cumulative coherence distributions were calculated for the following five Φ stress ratios: 0.0, 0.25, 0.5, 0.75 and 1.0. The resulting slip tendency of each theoretical fault was calculated along with the slip tendency distribution quartiles. The quartile values were used to create four fault population subsets: all data, and data with slip tendency greater than the first, the second and the third quartile respectively (Fig. 1). These simulations obviously provide only approximate models, inasmuch as all the factors regulating fault activities and their possible interactions are not yet completely understood (e.g. Nieto-Samaniego and Alaniz-Alvarez, 1997). The cumulative diagrams of the resulting distributions for both random movements and for the five considered Φ stress ratios are plotted in Fig. 2. While there is a high proportion of anti-coherent and incoherent pairs in a random population, incoherent and coherent pairs predominate in homogeneous stress field simulations, with coherent pairs favoured by high slip tendency values. Under stress fields with a stress ratio of about 0.5 the influence of slip tendency distribution is almost negligible. Another interesting result is the statistical equivalence of coherence distributions with Φ stress ratio values symmetric to 0.5 (i.e. 1.0 and 0.0, 0.75 and 0.25). Heterogeneous populations are expected to lie between the curves for homogeneous populations and those for random populations.

What information does coherence distribution provide? It is an objective measure independent of a-priori assumptions on the strain or stress field characteristics of a fault population. It can be used to test whether

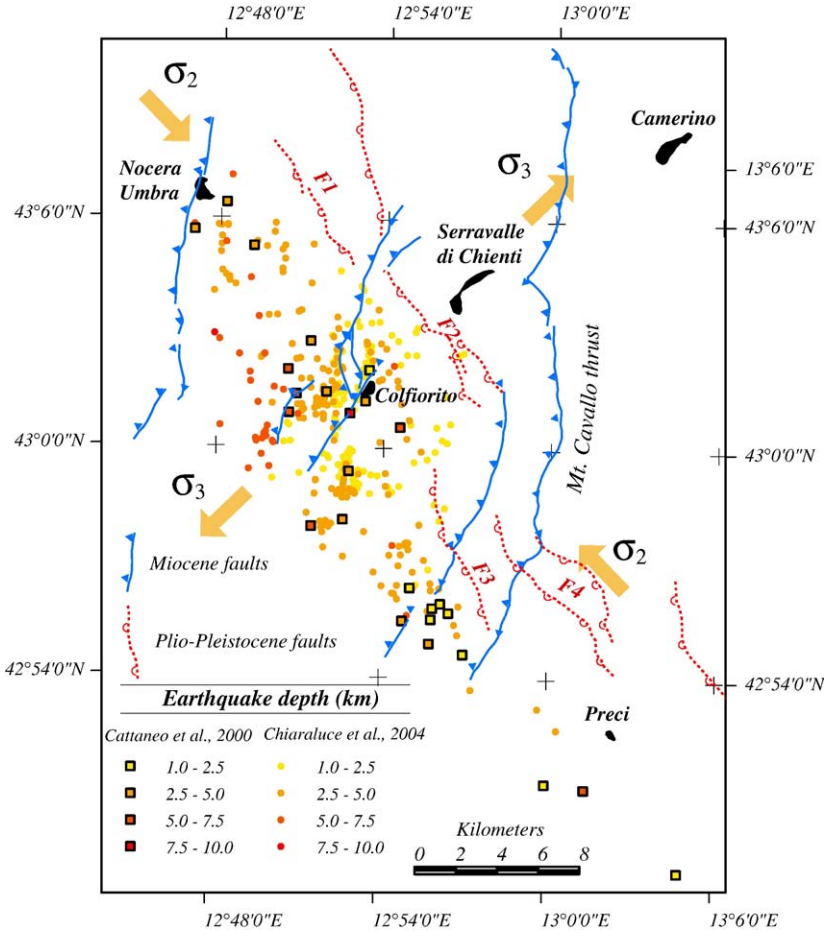

Fig. 4. Structural sketch map of the Colfiorito area, with seismic epicentres and normal faults activated during the seismic sequence according to Chiaraluce et al. (2005). Structural data redrawn from Figs. 3 and 6 in Chiaraluce et al. (2005), stress axes orientations derived from Chiaraluce et al. (2003).

observed populations, such as the ones previously described, conform to particular theoretical kinematic models. When determined along different directions, it can also provide information on the spatial isotropy or anisotropy of fault/earthquake populations.

3. Geological and seismotectonic settings of the 1997 Colfiorito–Sellano seismic sequence

The Colfiorito–Sellano seismic sequence developed in the Umbria–Marche sector of the northern Apennines. This sector was initially a marine basin which began to form in the Lias after the break-up of a continental craton. The eastward verging thrust-and-fold belt began to develop in the Late Cretaceous due to the collision between Adria and Europe (Dewey et al., 1989). Synsedimentary extensional events are recorded in the Jurassic and in the Cretaceous–Palaeocene (Lavecchia, 1985), and also just prior to the Miocene contractional phase (e.g. Scisciani et al., 2002). NW–SE to NNE–SSW trending thrusts and reverse-dextral faults with top-to-NE movements formed during the Miocene (Lavecchia, 1985; Lavecchia et al., 1994). The observed changes in fault directions have been ascribed to the local presence of oblique-lateral ramps (e.g. Koopman, 1983) or, based on palaeomagnetic analyses, to variations in strike due to folding of originally planar thrust surfaces (e.g. Dela Pierre et al., 1992). Starting in the

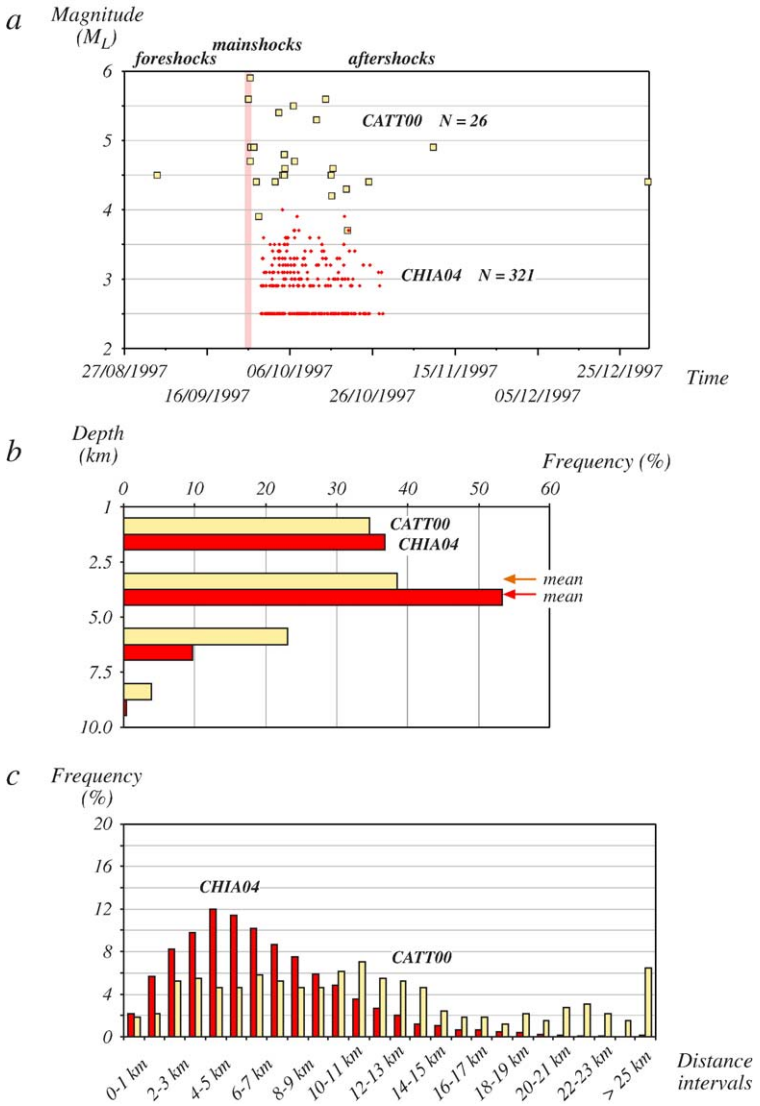

Fig. 5. Spatio-temporal characteristics of the two examined data sets: (a) time distribution vs. magnitude; (b) depth distribution; (c) distribution of spatial separation distances between seismic events.

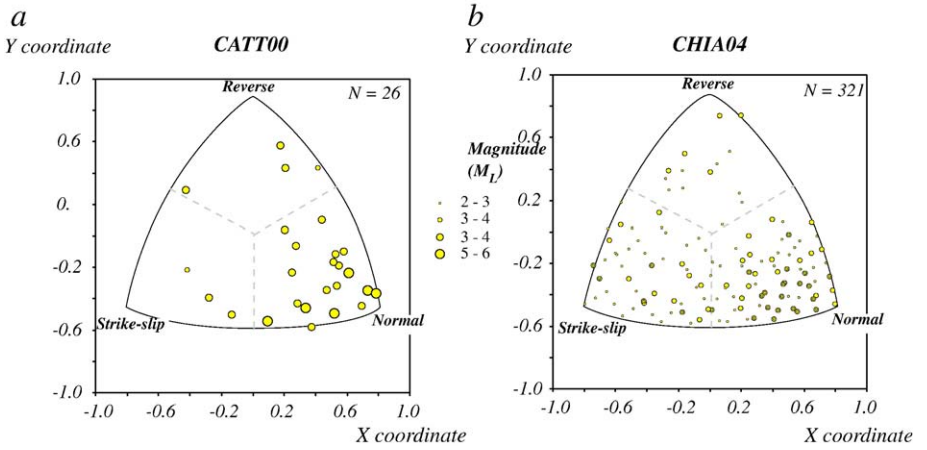

Fig. 6. Kinematic characteristics of the two examined seismic data sets, plotted using the method proposed by Kaverina et al. (1996): (a) CATT00 data set; (b) CHIA04 data set. Note the presence of normal, strike-slip and thrust events in both data sets.

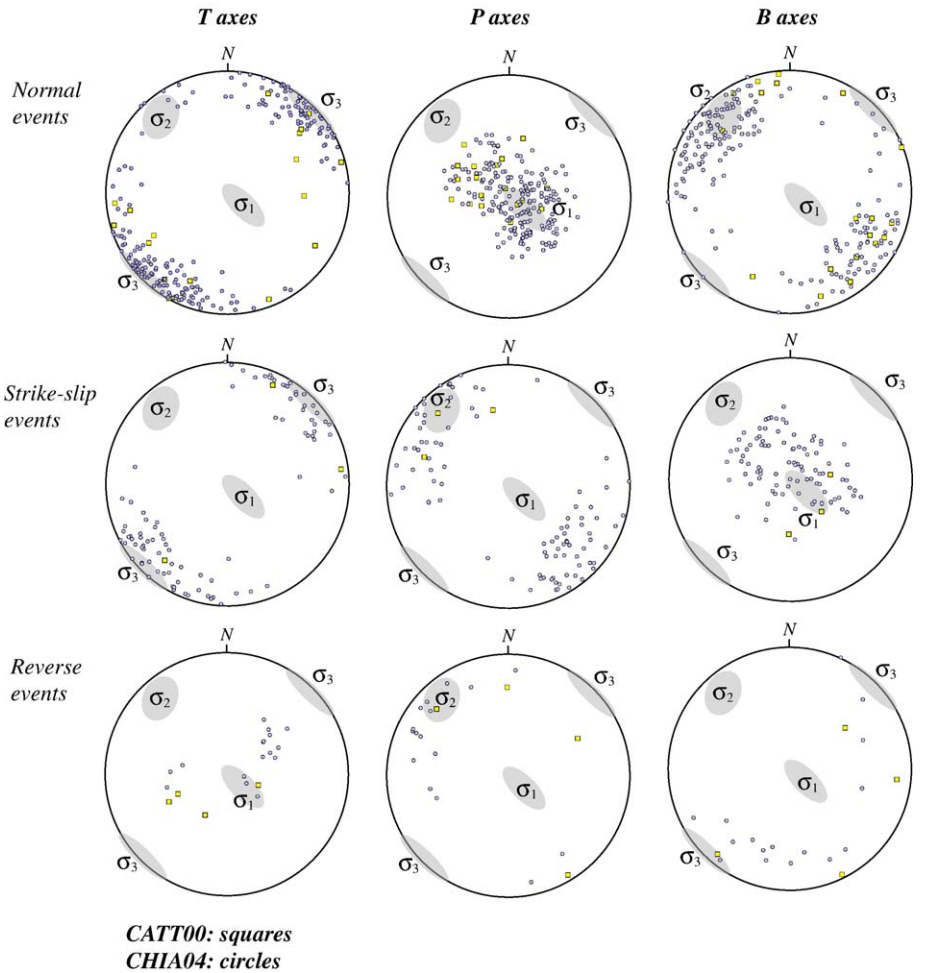

Fig. 7. Stereograms representing the orientation of *T*, *P* and *B* kinematic axes for normal, strike-slip and reverse events, as derived from the two data sets. Stress field orientations from Chiaraluce et al. (2003) are also shown.

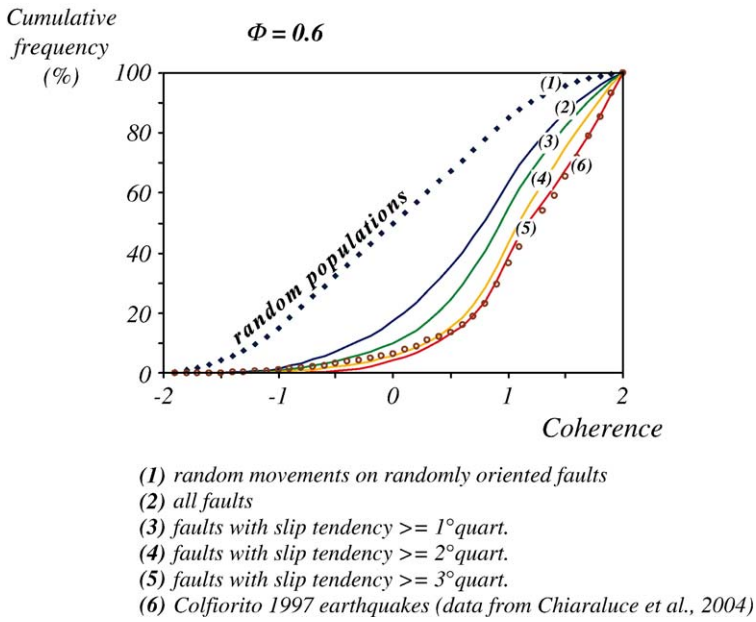

Fig. 8. Cumulative coherence distributions for a homogeneous stress field simulation (with stress ratio Φ=0.6), and for CHIA04 data set (empty circles). The best-fitting theoretical curve is that of slip tendency distributions greater than the third quartile.

Miocene the contractional phase gave way to an extensional phase. Extension began in the westernmost (Tyrrhenian) areas and extended progressively eastward, involving the Umbria–Marche sector in the Pliocene (Elter et al., 1975; Lavecchia et al., 1994). The present-day seismotectonic setting of the northern Apennines consists of two longitudinal belts with NE–SW extension in the internal, western zone and NE–SW compression in the external, eastern one (Fig. 3) (Lavecchia et al., 1994).

The Colfiorito–Sellano seismic sequence occurred in September–October 1997 in the area surrounding Colfiorito (Fig. 4). It was heralded by a foreshock on September 3rd (M_W=4.7), whereas the two main shocks

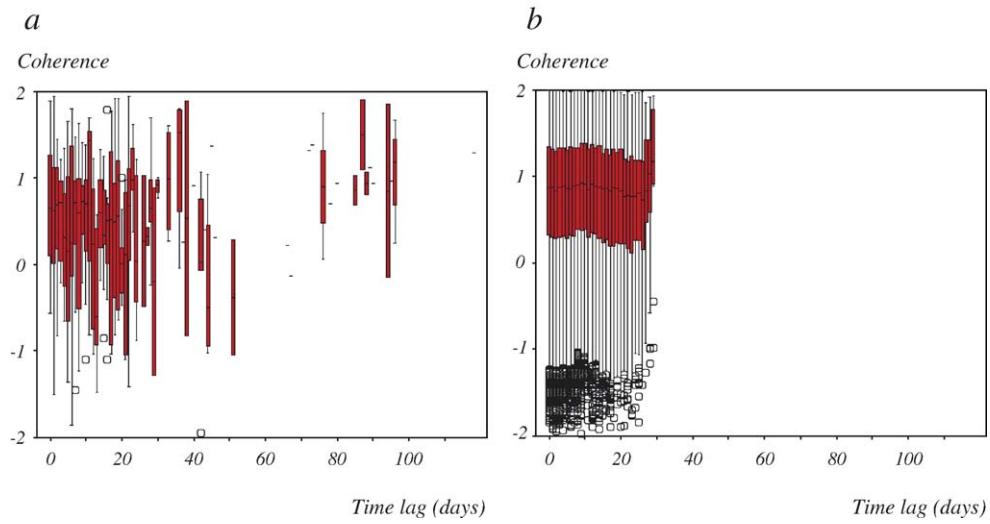

Fig. 9. Box plots of the coherence distribution with event pairs subdivided by time lag intervals: (a) CATT00 data set; (b) CHIA04 subset. Each box includes the range from the lower to the upper quartile, and the inner horizontal line represents the median. The vertical lines (whiskers) extend from the maximum to the minimum values that are not outliers, while circles and asterisks (where present) represent mild and extreme outliers, respectively (conventions also valid for Figs. 11, 13, 16, 18, 20).

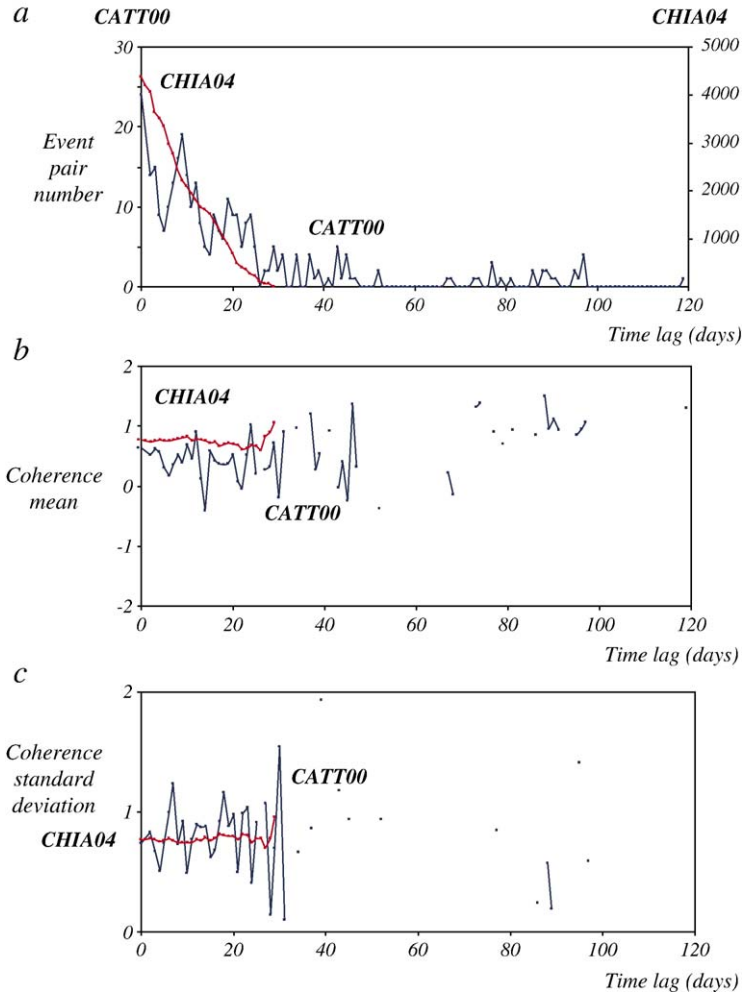

Fig. 10. Diagrams of coherence characteristics versus time lag intervals for the CATT00 and CHIA04 data sets: (a) number of event pairs; (b) coherence mean; (c) coherence standard deviation.

occurred in rapid succession on September 26th (M_W=5.7 and 6.0, at a 6 km depth, Amato et al., 1998; Ekström et al., 1998). After a period of relative quiescence, a subsequent minor seismic phase developed from February to April 1998 with low-magnitude normal events (Cattaneo et al., 2000; Morelli et al., 2000). Earthquakes were generally triggered in the uppermost 9 km, with the exception of two deep events which occurred at depths of 50–55 km (Cattaneo et al., 2000). The earthquakes developed in the Meso-Cenozoic carbonate unit and, from 6 km down, probably within the metamorphic basement (Chiarabba and Amato, 2003). The September–October 1997 events developed not only along three subparallel planes with a SW plunge and average dip of 40°–45°, but also along N–S trending discontinuities in the upper 2 km derived from the reactivation of pre-existing tectonic lineaments

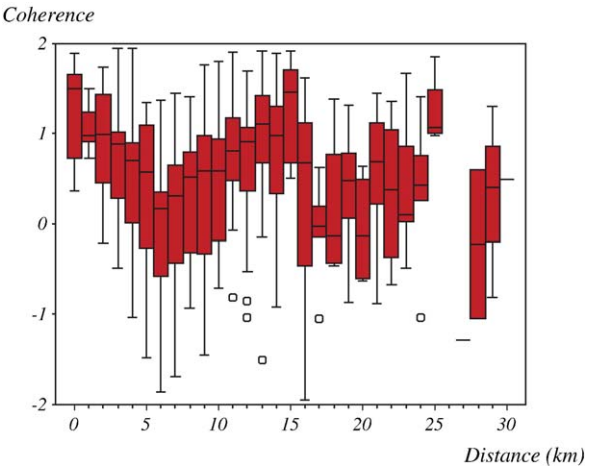

Fig. 11. Box plots of coherence versus separation between event pairs for CATT00 data set. Conventions as in Fig. 9.

(Cattaneo et al., 2000; Chiarabba and Amato, 2003; Chiaraluce et al., 2005; Collettini et al., 2005). Although the observed movements were mainly normal, i.e. congruent with the present-day normal faulting activity along NW–SE oriented faults (Ekström et al., 1998), strike-slip (about 1/4 of the total, mainly located near pre-existing N–S sub-vertical faults) and reverse movements (about 5%, showing no apparent spatial relationship to other structures) were also noted (Cattaneo et al., 2000; Chiaraluce et al., 2003). The direction of extension was oriented NE–SW in both the winter 1997 and spring 1998 seismic phases (Morelli et al., 2000). Based on the comparison between detailed maps of the terrain and seismic data, Chiaraluce et al. (2005) suggested that three of the major seismic events possibly originated along the surfaces of mapped Quaternary normal faults.

Chiaraluce et al. (2003) applied the Michael (1984) stress inversion technique to both the six major events and to the complete data set consisting of 321 data points. The resulting stress field is essentially homogeneous: the σ_3 axis is sub-horizontal with a NE–SW orientation, the σ_1 axis is sub-vertical, and the σ_2 axis is sub-horizontal to low-angle with a NW–SE orientation (see Fig. 4). The derived Φ stress ratio differs in the two cases: it is intermediate ($\Phi=0.6$) when considering the six main events only, but high ($\Phi=0.8$) when considering the entire data set. Comparison of stress inversion results with the local geology suggests that most focal mechanisms are congruent with present-day normal faulting activity (along NW–SE oriented faults), while a few events, mainly with strike-slip movements, strongly reflect the left-lateral reactivation of pre-existing N–S oriented strike-slip faults. The reverse events probably reflect minor local variations in the active stress field.

4. The influence of spatio-temporal parameters on kinematic and dynamic characteristics

This study was based on two distinct data sets deriving from published works (Cattaneo et al., 2000; Chiaraluce et al., 2004). These data sets were compiled by two research groups which operated independently during the seismic crisis. The first group, comprising the INGV (Istituto Nazionale di Geofisica e Vulcanologia) of Rome, GéoSciences Azur (France) and Camerino University, set up a temporary network of 26 digital seismic stations just after the two mainshocks (Amato et al., 1998). The second group had access to permanent regional networks (Marche, Abruzzo, Umbria) coordinated by the National Seismic Service (SSN), with a total of 40 digital seismic stations. These were integrated with a temporary network of 15 stations (Oct. 18–Nov. 3) and 12 strong motion stations (Oct. 3–May 1999) by the SSN and a group of research institutes under the aegis of the CNR-GNDT (National Research Council-National Group for Protection against Earthquakes) (Cattaneo et al., 2000). The two examined data sets, published in Cattaneo et al. (2000) and Chiaraluce et al. (2004), will be hereafter noted as CATT00 and CHIA04 respectively. The CATT00 data set consists of 26 focal solutions. Their positions derive from relocation using a depth-dependent 1-D model with station residual corrections; the mean standard deviation with respect to positions recorded by the temporary network (with estimated mean erh and erz of 0.2 km and 0.5 km respectively) is 1.3 km for depth and less than 1.0 km for horizontal. The formal errors in focal mechanisms,

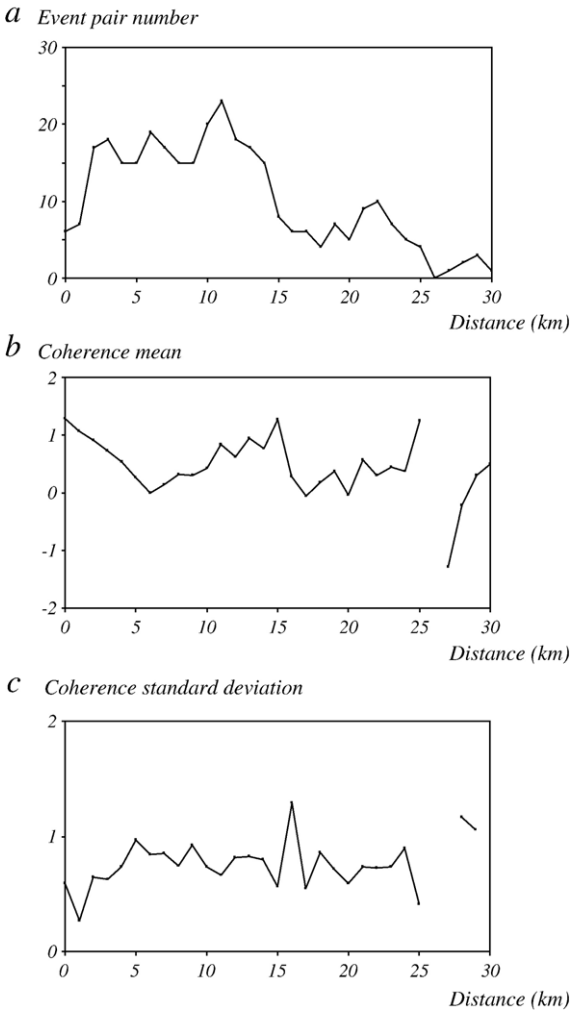

Fig. 12. Diagrams of coherence characteristics versus separation for the CATT00 data set: (a) number of event pairs; (b) coherence mean; (c) coherence standard deviation.

determined by the onset of P-wave polarities, are not reported. The CHIA04 data set consists of 321 focal solutions, with locations deriving from the tomographic inversion described in Chiarabba and Amato (2003), with mean formal errors in horizontal and vertical positioning of less than 0.5 km. The resulting formal errors in focal solutions are 10°, 15° and 30° for the strike, dip and rake angles, respectively. While the CHIA04 data set covers a one-month period starting 3 days after the two mainshocks, the CATT00 data set spans a period of about 4 months, although most events occurred in the month following the two mainshocks (Fig. 5a). Local magnitudes reported in CATT00 are higher than those in CHIA04. In both data sets most data derive from depths shallower than 5 km; only the CATT00 data set contains a significant number of data points from greater depths (Fig. 5b). The distance between events is predominantly less than 10 km for CHIA04, with a mode of 5 km. For CATT00 the distribution is quite uniform in the 2–15 km interval, with a significant number of events more than 20–25 km apart (Fig. 5c).

Focal mechanisms are visualized using the equal-area projection of a sphere octant (Fig. 6), as proposed by Kaverina et al. (1996). Focal mechanism characteristics vary greatly in both examined data sets, as noted in Cattaneo et al. (2000) and Chiaraluce et al. (2004). Normal events predominate in both number and magnitude, and show a continuous transition to strike-slip events. Reverse events are also present in both data sets. There is a decrease in the maximum magnitude of events from normal to strike-slip and reverse events (Fig. 6). The *T*, *P* and *B* kinematic axes from the two data sets are projected in the stereograms of Fig. 7 according to the three movement types (normal, strike-slip and reverse, as defined in Fig. 6). Stress field orientations from Chiaraluce et al. (2003) are also shown for comparison. The kinematic axis orientations of the two data sets are in good agreement; however, the smaller CATT00 data set tends to be more dispersed. *T* axes mostly indicate sub-horizontal extension in a NE–SW direction, i.e. parallel to the derived σ_3, although some data are dispersed along the $\sigma_2-\sigma_3$ plane or, in the case of reverse earthquakes, along the $\sigma_1-\sigma_3$ plane. While *P* axes are sub-vertical for normal earthquakes, they suggest a low-angle NW–SE shortening direction for both strike-slip and reverse events. The orientation of the neutral axis tends to be less defined than that of the other two axes: it is mainly NW–SE for normal events, sub-vertical for strike-slip events, and quite dispersed for reverse events.

To test the hypothesis of stress field homogeneity proposed by Chiaraluce et al. (2003), the coherence distribution for the complete CHIA04 data set was compared to the theoretical distributions shown in Fig. 2. This comparison indicates that the distribution of the complete earthquake data set is compatible with a homogeneous field characterized by a Φ stress ratio of 0.5 ± 0.25. The Φ stress ratio of 0.60 calculated by Chiaraluce et al. (2003) was then used to derive the best-fitting slip tendency distribution for this data set: the observed distribution fits the third quartile of slip tendency in the 1–2 coherence interval well, particularly

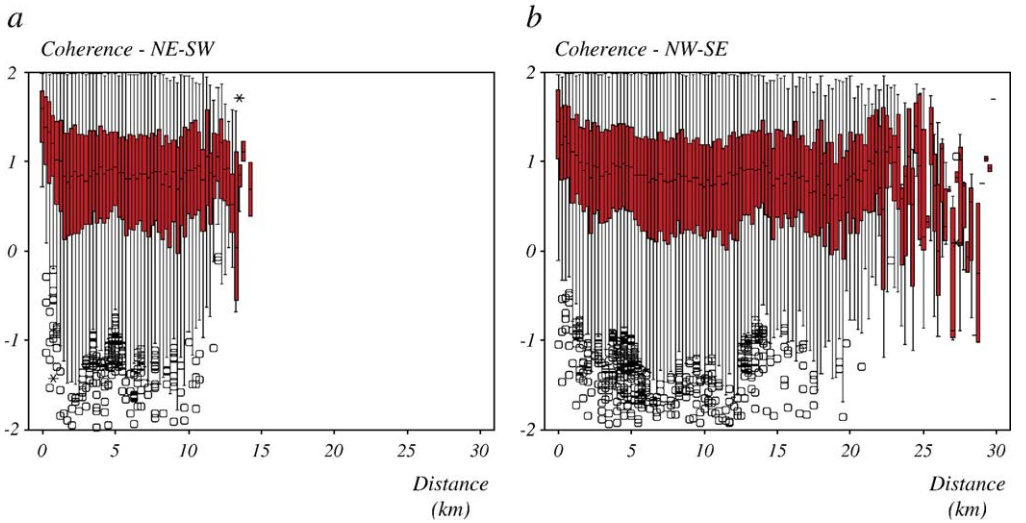

Fig. 13. Box plots of the spatial dependence of coherence for two CHIA04 subsets (considering only the event pairs connected by vectors dipping less than 45°): (a) pairs with directions falling in the NE–SW quadrant (0°–90° orientation interval); (b) pairs with directions falling in the NW–SE quadrant (90°–180° orientation interval). Conventions as in Fig. 9.

in the 0.5–2.0 range (Fig. 8). However, for lower coherence values the empirical distribution intersects the second and even the first slip tendency quartile, showing higher than expected proportions of incoherent and anti-coherent earthquake pairs. This discrepancy could be related to the presence of a high proportion of pre-existing surfaces sub-perpendicular to a principal stress axis or, alternatively, the low coherence values could reflect a certain degree of stress heterogeneity.

4.1. Time dependence

While the time-coherence relationships for the CATT00 data set are quite erratic, probably due to the low number of available events, they are better defined for the CHIA04 data set (Figs. 9 and 10). The median and mean values of coherence for both data sets are slightly less than 1.0 (lower for CATT00 than for CHIA04), as are the standard deviations of coherence. Values do not appear to be significantly influenced by the increasing time lag.

4.2. Distance dependence

Coherence statistics were analyzed with respect to the 3D separation distance between earthquake pairs. The coherence values in the CATT00 data set present an apparent spatial cyclicity, as evidenced by variations in the mean, median and extreme values, which tend to decrease for the first 7 km, then increase up to 14 km and subsequently show at least two other increase–decrease trends (Figs. 11 and 12). The observed period is of about 14 km and the amplitude is greater than 1.0. However, the low number of available seismic events (26 events) could possibly reduce the statistical significance of results and did not allow directional analysis for the detection of spatial anisotropies. The larger CHIA04 data set has greater statistical significance and enables directional analysis in NE–SW (i.e. sub-perpendicular to the normal faults) and NW–SE directions (i.e. sub-parallel to the normal faults and sub-perpendicular to the Miocene reverse faults): event pairs with connecting vectors inclined more than 45° are filtered out to highlight the directional influence (Figs. 13 and 14). The main characteristics of relationships between coherence and spatial separation are:

a) in the first separation interval (0–1 km) coherence mean and median values consistently present the highest statistically significant values;
b) the mean and median coherence decrease rapidly in the 0 to 2–3 km interval;
c) values in both subsets tend to slowly decrease from 2–3 km to 10 km;
d) the standard deviation of coherence increases in the first 3 km of separation (i.e. in this range the series are heteroscedastic), while it appears to be almost constant (i.e. the series are homoscedastic) for greater distances.

Coherence variations differ in the two directions of analysis: the rate and total magnitude of variations are

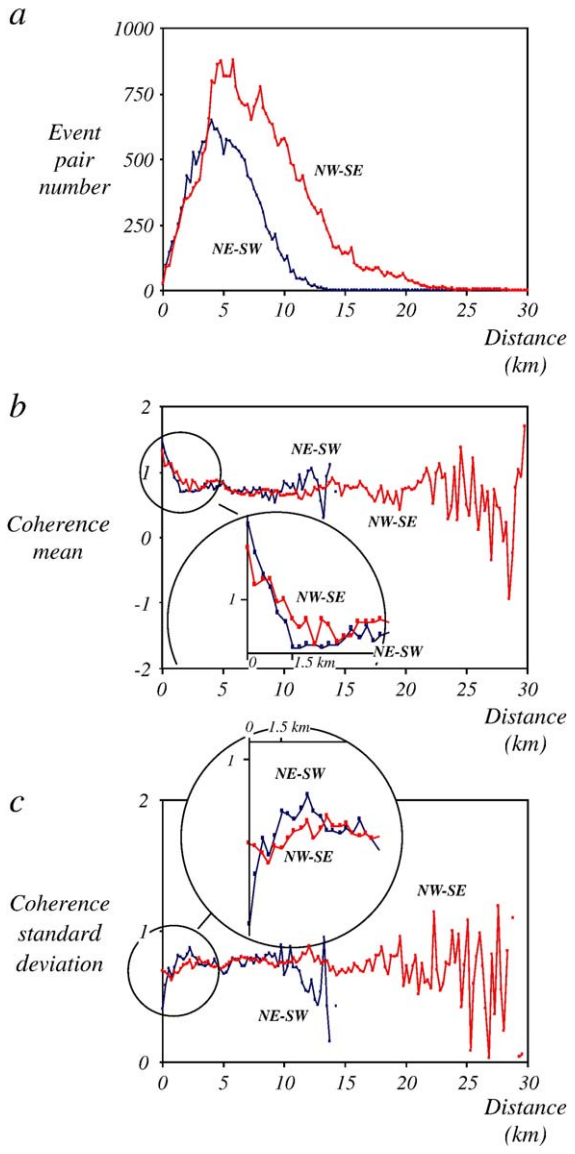

Fig. 14. Diagrams of coherence vs. distance for NE–SW (0°–90° orientation interval) and NW–SE (90°–180° orientation interval) CHIA04 subsets: (a) number of event pairs; (b) coherence mean; (c) coherence standard deviation.

higher in the NE–SW direction of analysis than in the NW–SE direction (insets in Fig. 14b, c).

4.3. Depth influence

Chiaraluce et al. (2004) noted that the depth parameter plays a significant role in determining the earthquake type: reverse and strike-slip events are prevalently located in the uppermost 2 km, whereas normal events tend to predominate with increasing depth. To investigate the influence of depth on the seismic sequence, kinematic axis orientations for three depth intervals were plotted in separate stereograms (Fig. 15), and kinematic components were plotted against depth (Fig. 16). In the first 2.5 km the *T* axes are clustered in a sub-horizontal NE–SW direction (with some sub-vertical data), while in the 2.5–5.0 km interval they are more scattered along the sub-horizontal plane, with some data describing a NW–SE trend. The *P* axes are distributed along a sub-vertical NW–SE plane in the shallower depth interval, while they tend to become sub-vertical in the deeper sectors. *B*-axes are the kinematic axes with the most scattered orientations; like the *P* axes, they lie along a sub-vertical NW–SE plane, and their plunge decreases with depth.

The normal component tends to increase from 1 km to almost 3.5 km, and then remains almost constant (Fig. 16a; note that the observed trend for distances larger than 4.5 km may not be statistically significant due to the low number of data points). The median value of the reverse component does not show any particular trend, but extreme values are more frequent in the first 2.5 km (Fig. 16b).

In conclusion, most events indicate a gradual transition from superficial tectonics (in the shallowest

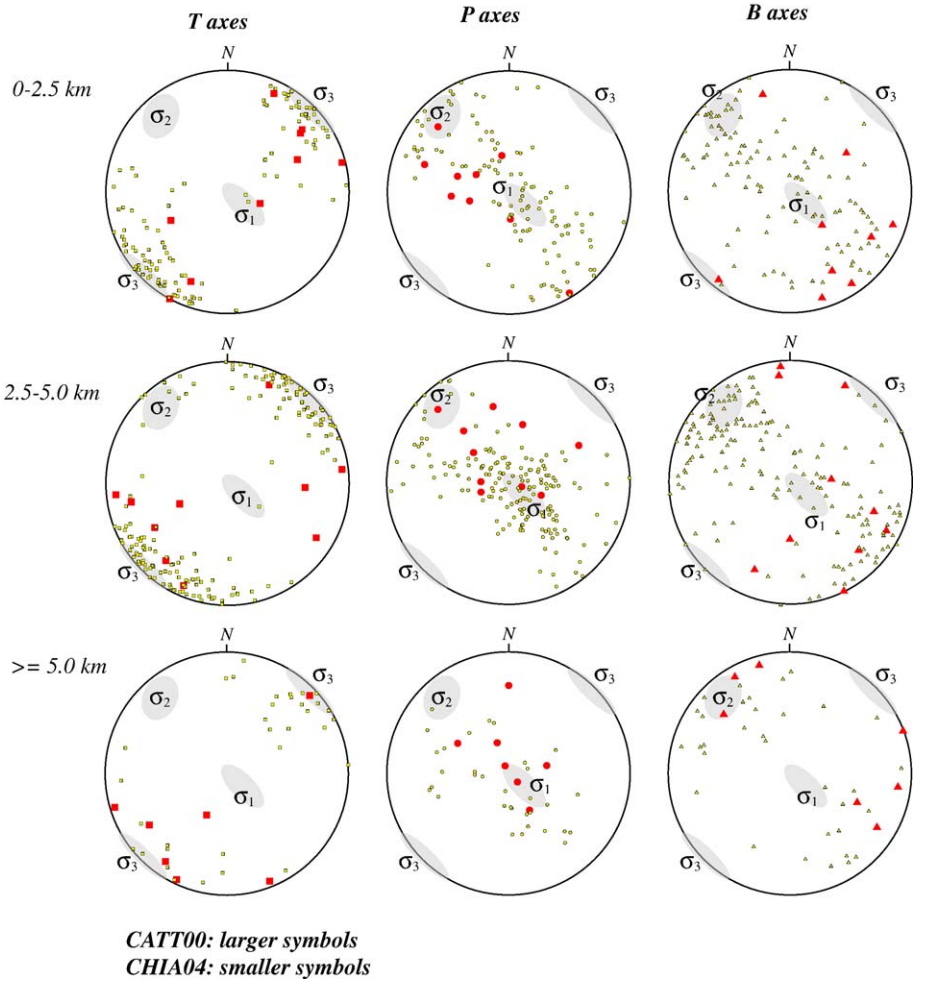

Fig. 15. Stereograms of *T*, *P* and *B* kinematic axes for three different depth slices (0–2.5 km, 2.5–5.0 km, and deeper than 5.0 km), as derived from the two data sets. Stress field orientations from Chiaraluce et al. (2003) are also shown.

2–3 km) characterized by extension/transtension in a NE–SW direction, with a marked tendency to exchange the orientation between *P* and *B* axes, to deeper tectonics with prevailing tension and a more dispersed sub-horizontal extension direction.

4.4. Relationships with pre-existing lineaments

To investigate the spatial relationships between pre-Pliocene NNE–SSW trending faults and movement type, GIS software was used to create a distance map of the pre-Pliocene faults mapped in Chiaraluce et al. (2005, Figs. 3 and 6) (Fig. 17). Considering that a sub-vertical attitude of the pre-Pliocene faults is consistent with available seismic data (e.g. Chiaraluce et al., 2005), a 2D distance map can be an effective tool for investigating spatial relationships between seismic events and pre-Pliocene faults. Results obviously depend on the completeness of fault mapping, which decreases with their decreasing importance. Correlation tests on the CHIA04 data set revealed no particular relationship between distance from the pre-Pliocene faults and earthquake magnitude. However, there seems to be some correlation between the kinematic components of events and the relative distance from pre-Pliocene faults. As seen in Fig. 18a, the *X* parameter (sensu Kaverina et al., 1996), which expresses the relative predominance of strike-slip (negative values) or normal (positive values) components, tends to increase in the 0–3 km interval: the strike-slip component is more important near the oblique pre-Pliocene faults and diminishes with distance from the faults. Due to the low number of data in that interval, the observed decrease for distances greater than 3 km may not be statistically significant. The relationship observed in the first 2 km of separation suggests that strike-slip movements mainly originate near pre-Pliocene faults, confirming findings in Chiaraluce et al. (2004, 2005) and Collettini et al. (2005). The *Y* parameter, which expresses the importance of the reverse component with respect to the two other components, suggests a positive correlation between pre-Pliocene faults and reverse components of movement occurring up to over 1 km from faults: data with high *Y* values are more frequent in the first km of

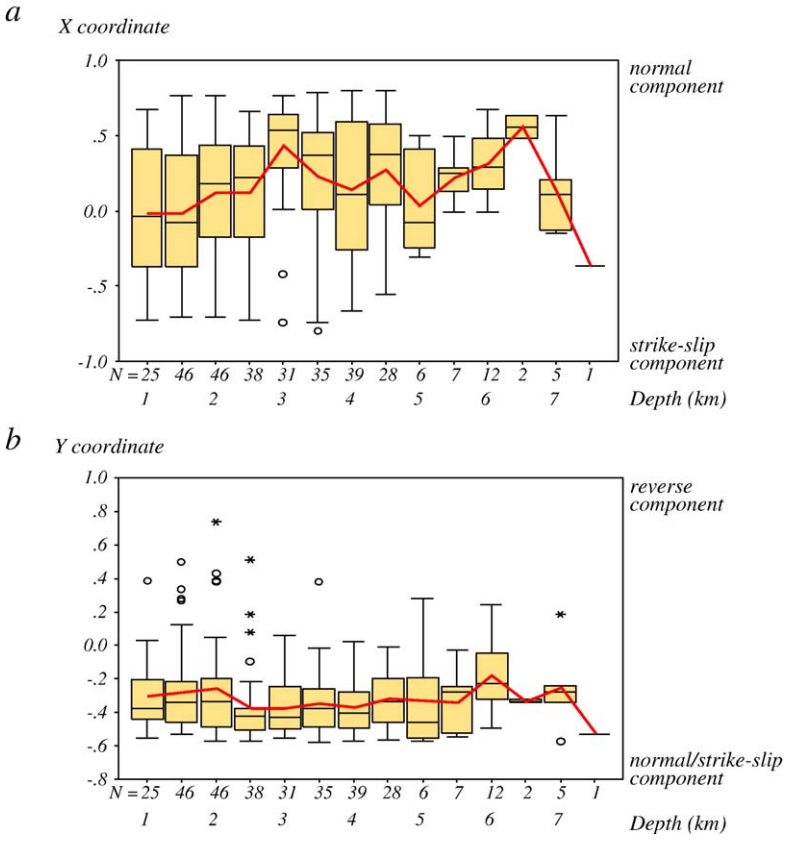

Fig. 16. Box plots of kinematic components of seismic events (obtained following the method of Kaverina et al., 1996) vs. depth, for CHIA04 data set: (a) *X* coordinate: normal vs. strike-slip components; (b) *Y* coordinate: reverse vs. normal/strike-slip components. Conventions as in Fig. 9.

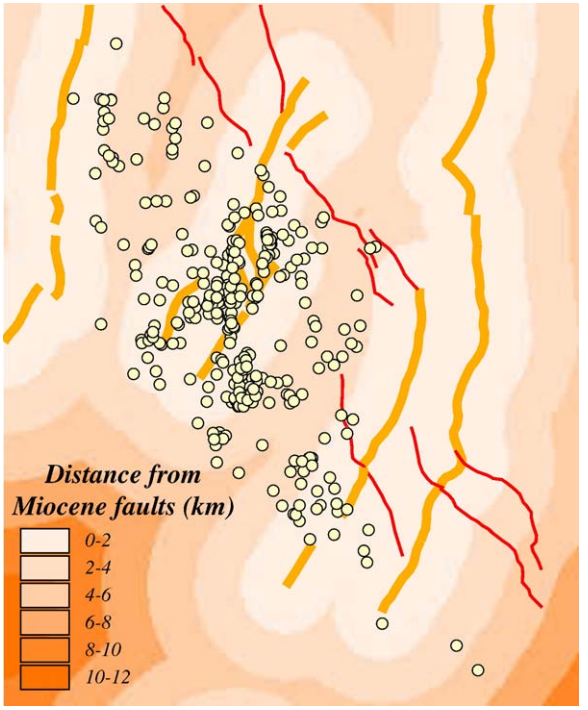

Fig. 17. Map of the 2D distance of seismic events from the pre-Pliocene NNE–SSW trending lineaments (thick lines).

separation (Fig. 18b). These findings suggest that both strike-slip and reverse movements are favoured by the vicinity of pre-existing oblique faults, as well as by shallow depths (cf. Figs. 16 and 18).

5. Discussion

5.1. Considerations on the stress field

The results of spatial analysis (see Figs. 11–18) indicate that pre-existing discontinuities may influence the movement type of earthquake events: in an extensional setting, reactivated oblique lineaments may favour the activity of strike-slip and thrust faults. Distance from the oblique lineaments appears to control the proportion of normal vs. strike-slip and reverse events (Fig. 18), with a gradual decrease in non-normal events with increasing distance from the oblique lineaments (after 2.5–3.0 km the importance of normal movements appears to decrease, but this may not be a statistically significant finding). Nostro et al. (2005) revealed that an increase in Coulomb stress after the normal earthquakes could have promoted strike-slip events along the pre-existing oblique lineaments, thus providing evidence for interplay between kinematic and static factors. The relative importance of these two factors could be better defined through further investigation. When applying classic stress inversion techniques (e.g. Angelier, 1984) the presence of mixed data types (i.e. strike-slip, normal and reverse faults) does not automatically imply a polyphase history. A fraction of data may show a certain degree of kinematic and dynamic inconsistency within a single tectonic phase if pre-existing discontinuity surfaces were reactivated. The analysis of quantitative spatial relations between kinematic characteristics and tectonic lineaments (for example through GIS techniques) can help distinguish between the role of spatial kinematic heterogeneities and that of temporal variations in stress fields. Moreover, changes in the depth of analyzed structures may also be accompanied by kinematic variations in faults.

5.2. How significant are the coherence variations?

As the previous analyses show, the spatial factor is an important factor controlling the kinematic similarity between seismic events. It is more important than time,

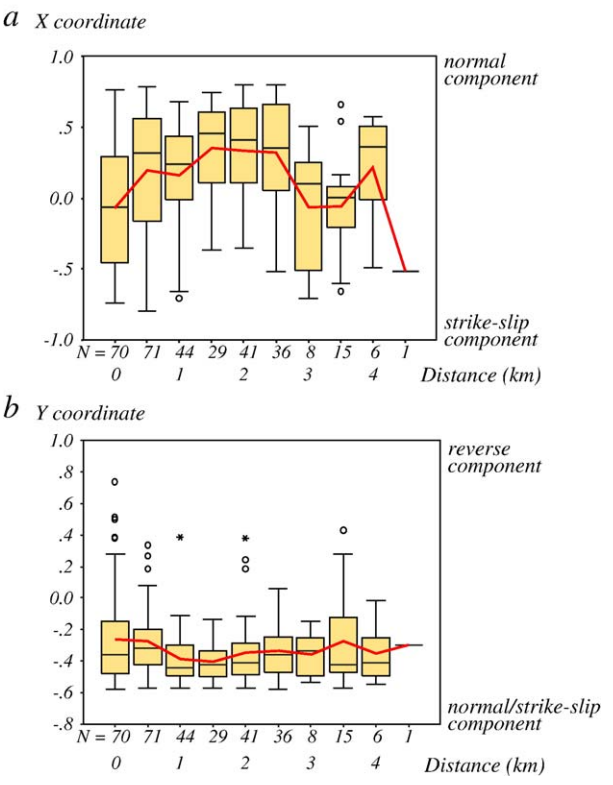

Fig. 18. Box plots of the kinematic parameter values (sensu Kaverina et al., 1996) vs. distance from the pre-Pliocene NNE–SSW trending lineaments, for CHIA04 data set: (a) *X* coordinate: normal vs. strike-slip components; (b) *Y* coordinate: reverse vs. normal/strike-slip components. Conventions as in Fig. 9.

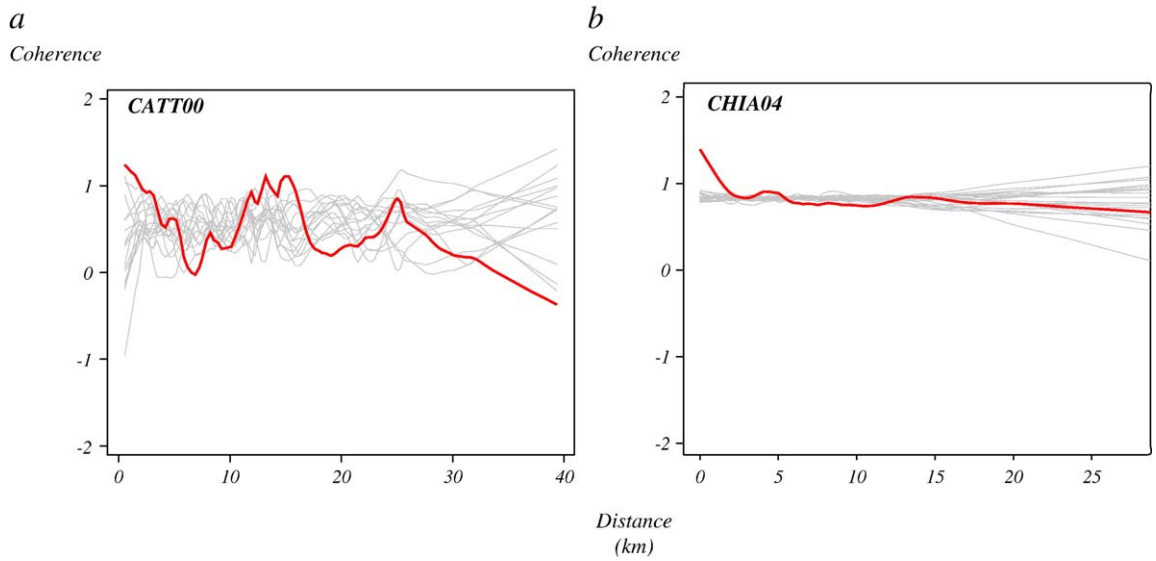

Fig. 19. Diagrams representing the reshuffled (grey) versus the natural (red) smoothed values of coherence for the CATT00 (a) and the CHIA04 data set (b). (For interpretation of the references to colour in this figure legend, the reader is referred to the web version of this article.)

as indicated by the absence of marked coherence variations for increasing time lags (even when taking into account the different lengths of time covered by the two data sets) and by the lower mean coherence between events when grouping according to time rather than spatial separation (compare Fig. 10b with Fig. 14b).

As described earlier, the two analyzed data sets have different original characteristics (i.e. number of focal mechanisms, processing methodologies) and show quite different spatial variations, with an apparent cyclicity in the case of the CATT00 data set (Figs. 11 and 12). However, we cannot exclude that the observed variations are casual (due to the small size of the data set) and do not represent real spatial variations. Classical statistical tests of significance assume independence between observations; they are thus difficult to apply here, as many different coherence values derive from a single focal mechanism. An alternative approach for testing the significance of spatial variations consists in generating artificial data sets through random permutations of the

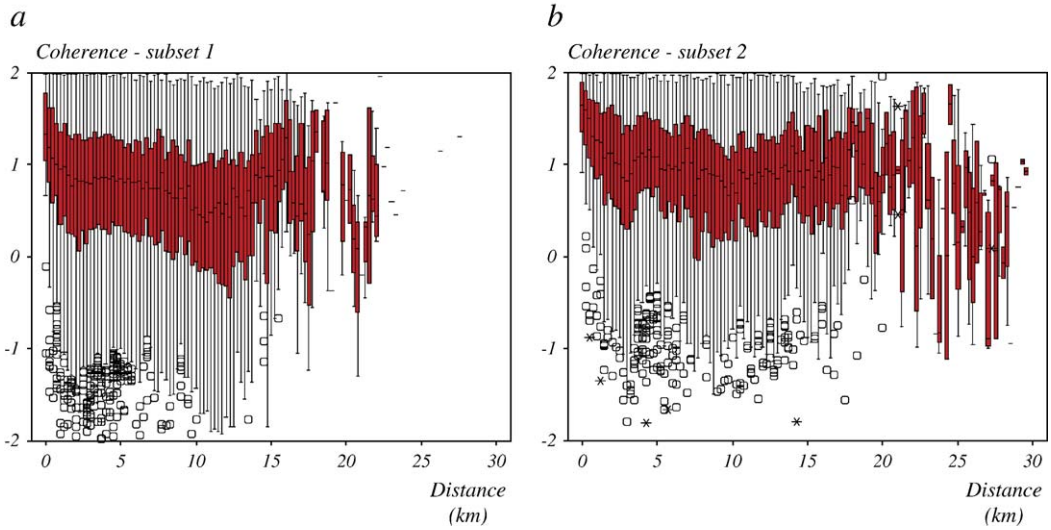

Fig. 20. Box plots of coherence vs. separation for two spatial subsets of CHIA04 data set: (a) subset 1—pairs with both events located within a 1.5 km-distance threshold from the pre-Pliocene NNE–SSW trending lineaments; (b) subset 2—pairs with both events outside the 1.5 km-distance threshold. Conventions as in Fig. 9.

observed locations between the different events which destroy any non-random spatial coherence variations (the "reshuffling" procedure described in Huc and Main, 2003). Natural variations with amplitudes much larger than those observed for an adequate number of randomly-reshuffled data may be considered non-casual and thus seismologically significant. Twenty reshuffled data sets were calculated for both the CATT00 and the CHIA04 data sets, and the smoothed values of coherence are compared to the natural ones in Fig. 19. For the CATT00 data set, the maximum amplitudes of the average coherence variations are of the same magnitude as those of the reshuffled data (Fig. 19a): the natural variations are thus not considered to be statistically significant. On the other hand, for the CHIA04 data set the average coherence in the first 2 km of separation differs markedly from that of reshuffled data (Fig. 19b). These analyses suggest that coherence variations may be considered significant only when there is sufficient data (at least some hundreds of data points) and when locations have small positional errors (at least with respect to the investigated distance interval).

5.3. What determines the decrease in similarity with increasing distance?

As discussed in the preceding paragraph, the decay of kinematic correlation between faults in the first 2 km of separation appears to be of seismological and/or geological significance. This fast initial decay may result from factors such as the presence of pre-existing lineaments, which appear to influence the kinematic characteristics of events (cf. Fig. 18). To test this hypothesis, the CHIA04 data set was partitioned into two subsets: events occurring within 1.5 km of the Miocene faults, and those occurring at distances greater than 1.5 km. If the initial rapid decrease in coherence is mainly due to the influence of the Miocene faults, the two subsets should show distinctly different rates of decrease in the first km of separation, with a lower rate for the second subset. This does not appear to be the case, as may be deduced from Figs. 20 and 21. The mean values of pairs located more than 1.5 km from the Miocene faults are greater than in the other subset (due to the higher complexity of faults in proximity to the Miocene faults), but the decrease rates observed in the initial kilometres of separation for the two subsets are almost equivalent. Although this result seems to exclude that pre-existing faults are responsible for the initial rapid decrease in coherence, it reveals their importance in the overall kinematic process.

The results of the various spatial analyses are plotted in log-linear diagrams (Fig. 22) together with other data compiled from Kagan's works (Kagan and Knopoff, 1985b; Kagan, 1992a). Note that the absolute values of the average coherence vary from data set to data set mainly as a function of the considered range in earthquake magnitude (as in the data from Kagan's works) or as a function of the structural complexity of the analyzed zones (e.g. cases D and E in Fig. 22). In the 200–20,000 m interval the two CHIA04 subsets, defined according to the distance from the pre-existing faults (cases D and E in Fig. 22), present similar, broadly constant decreasing trends that are much like those derived from the California and worldwide earthquake catalogues (cases A–C, from Kagan and Knopoff,

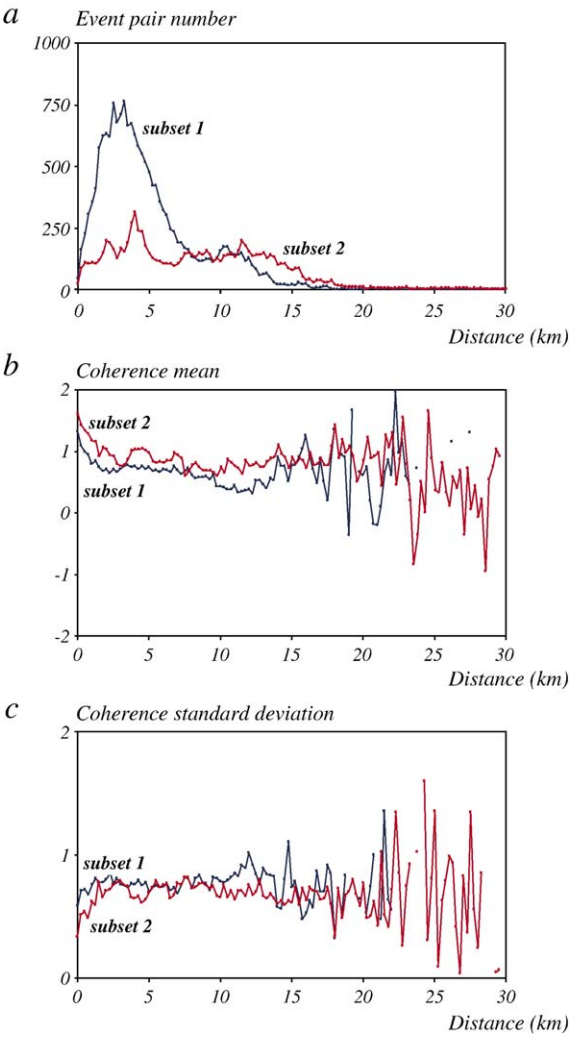

Fig. 21. Statistics of the coherence distribution for CHIA04 spatial subsets as in Fig. 20: (a) event pair number; (b) coherence mean; (c) coherence standard deviation.

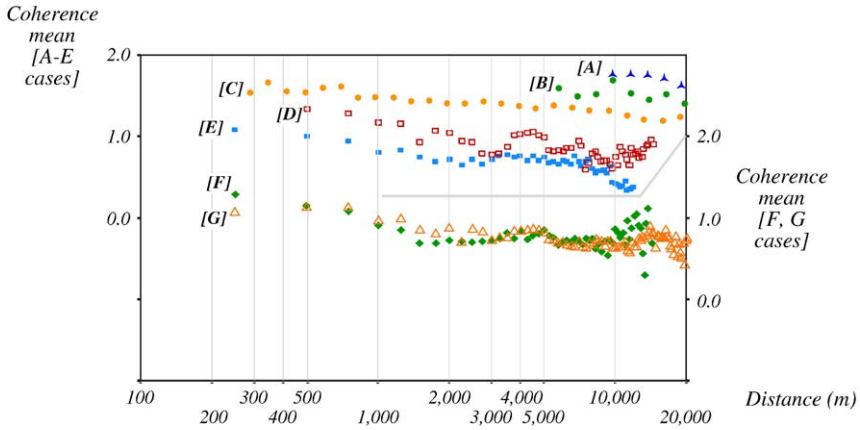

[A] Harvard catalogue, 0-70 km depth, Mw >= 6.0 (N= 1457), Kagan, 1992a, Fig. 3b.

[B] Harvard catalogue, 0-70 km depth, Mw >= 5.0 (N= 6392), Kagan, 1992a, Fig. 3a.

[C] USGS average Coyote & Eastbay cats. (Calif.), ML >= 1.5 (N= 841), Kagan and Knopoff, 1985b, Fig. 6.

[D] CHIA04 event pairs located outside a 1.5 km distance from pre-existing faults (subset 2 in Figs. 19, 20) (only intervals with number of cases > 100)

[E] CHIA04 event pairs located within 1.5 km from pre-existing faults (subset 1 in Figs. 19, 20) (only intervals with number of cases > 100)

[F] CHIA04 directional analysis: NE-SW subset (cf. Figs. 13, 14).

[G] CHIA04 directional analysis: NW-SE subset (cf. Figs. 13, 14)

Fig. 22. Log-linear diagram of coherence vs. separation for data sets compiled from literature (sets A and B from Kagan, 1992a; set *C* from Kagan and Knopoff, 1985b; modified after Fig. 8 in Alberti, 2006) and from this study (subsets D and E, cf. Figs. 20 and 21, subsets F and G correspond to the NE–SW and NW–SE subsets respectively, as in Figs. 13 and 14).

1985b; Kagan, 1992a). In contrast, the two subsets defined according to NE–SW or NW–SE directions of analysis (cases F and G) do not have similar decreasing trends, as already noted in paragraph "4.2 Distance dependence". For NE–SW directions (i.e. perpendicular to the normal faults), coherence decreases quickly up to separation distances of 1500 m and then remains almost constant, while for NW–SE directions the decrease rate is lower and does not change abruptly at 1500 m. As a result, we infer that the normal fault architecture could be the main factor controlling the behaviour of coherence in the first kilometres of separation as well as the genesis of directional anisotropies. In Fig. 4 the mean along-dip separation between the normal faults is about 2 km, i.e. similar to the separation value at which there is a marked change in the decrease rate of coherence. The along-dip spatial separation in fault systems could be the specific factor regulating the kinematic similarity in seismic events. To confirm this hypothesis, other data sets with different along-dip separation values should be examined.

In conclusion, while the local structural complexity of earthquakes in the Colfiorito–Sellano seismic sequence appears to be controlled by the variable orientation of discontinuity surfaces, the similarity decrease rate is possibly regulated by the architecture of the neo-formed geological faults, and consequently by the active stress field and the anisotropic mechanical characteristics of the medium.

6. Conclusions

Temporal and spatial analyses of coherence, a kinematic parameter that expresses the similarity between earthquakes (Kagan and Knopoff, 1985a,b; Kagan, 1992a), were completed on two published data sets on the 1997 Sellano–Colfiorito normal faulting seismic sequence (Cattaneo et al., 2000; Chiaraluce et al., 2004) which affected the northern Apennine polyphase sedimentary terrains. Reshuffling tests performed on the two data sets with a marked difference in the number and locational precision of reported events reveal the importance of these two factors in obtaining statistically significant results from coherence analyses: large data sets (with at least some hundreds of events) with low locational errors are required. The results from the data set fulfilling these requirements, i.e. that of Chiaraluce et al. (2004), reveal the presence of a fast initial decrease in coherence associated with an anisotropic kinematic structure. Kinematic similarity is

high for short separation distances between events (i.e. <1 km) but decreases quickly in the first 2 km of separation, particularly in the direction perpendicular to the strike of normal faults. The decrease rate is much lower for larger distances. This behaviour is possibly controlled by the structure of the normal fault segments (with a mean along-dip separation distance of 2 km), which depends on the stress field and the mechanical characteristics of the deformed rock volumes. The proximity (within 1–2 km) to high-angle faults that are oblique to the normal faults and derive from the previous compressional phase, appears to significantly lower similarity values through the activation of strike-slip and reverse fault planes. The presence of high-angle faults, however, does not influence the similarity decrease rate. These faults possibly experienced kinematic inversion from reverse-dextral in the Miocene to left-lateral-normal starting in the Plio-Pleistocene, in response to a change in tectonic regime from transpression to extension (Lavecchia, 1985; Chiaraluce et al., 2003, 2004). The analyzed seismic sequence demonstrates that earthquake populations in regions characterized by the presence of inherited faults may present mixed fault types (i.e. normal, strike-slip or reverse). The spatial analysis of fault populations, particularly of their relationship with geological macro-structures, may help interpret the results of stress inversion analyses. Spatial analysis may help establish whether kinematically different events should be ascribed to different diachronic tectonic phases or to a single phase characterized by spatial heterogeneity due to, for example, the reactivation of pre-existing faults.

Acknowledgements

This work was possible thanks to the availability of the Cattaneo et al. (2000) and Chiaraluce et al. (2004) data sets. GIS processing was completed at the GIS-RS Laboratory of MNA-Siena. The customized ArcView® 3.1 GIS project is available from the author upon request. Stereoplots for rotation pole analyses were created using a modified version of the Knox-Robinson and Gardoll (1998) ArcView customization. A. Palladino is thanked for the revision of the English.

References

Alberti, M., 2005. Application of GIS to spatial analysis of mesofault populations. Computers & Geosciences 31, 1249–1259. doi:10.1016/j.cageo.2005.03.013.

Alberti, M., 2006. Spatial structures in earthquakes and faults: quantifying similarity in simulated stress fields and natural data sets. In: Lisle, R.J., Blenkinsop, T.G. (Eds.), Special Issue on "New Dynamics into Palaeostress Analysis". Journal of Structural Geology, vol. 228, pp. 998–1018. doi:10.1016/j.jsg.2006.03.017.

Amato, A., Azzara, R., Chiarabba, C., Cimini, G.B., Cocco, M., Di Bona, M., Margheriti, L., Mazza, S., Mele, F., Selvaggi, G., Basili, A., Boschi, E., Courboulex, F., Deschamps, A., Gaffet, S., Bittarelli, G., Chiaraluce, L., Piccinini, D., Ripepe, M., 1998. The 1997 Umbria–Marche, Italy, earthquake sequence: a first look at the main shocks and aftershocks. Geophysical Research Letters 25, 2861–2864.

Angelier, J., 1984. Tectonic analysis of fault slip data sets. Journal of Geophysical Research 89 (B7), 5835–5848.

Bott, M.H.P., 1959. The mechanics of oblique slip faulting. Geological Magazine 96, 109–117.

Cattaneo, M., Augliera, P., De Luca, G., Gorini, A., Govoni, A., Marcucci, S., Michelini, A., Monachesi, G., Spallarossa, D., Troiani, L., XGUMS, 2000. The 1997 Umbria–Marche (Italy) earthquake sequence: analysis of the data recorded by the local and temporary networks. Journal of Seismology 4, 401–414.

Cello, G., Mazzoli, S., Tondi, E., Turco, E., 1997. Active tectonics in the central Apennines and possible implications for seismic hazard analysis in peninsular Italy. Tectonophysics 272, 43–68.

Chiarabba, C., Amato, A., 2003. V_p and V_p/V_s images in the M_w 6.0 Colfiorito fault region (central Italy): a contribution to the understanding of seismotectonic and seismogenic processes. Journal of Geophysical Research 108 (B5), 7/1–17. doi:10.1029/2001JB001665.

Chiaraluce, L., Ellsworth, W.L., Chiarabba, C., Cocco, M., 2003. Imaging the complexity of an active normal fault system: the 1997 Colfiorito (central Italy) case study. Journal of Geophysical Research 108 (B6), 2294. doi:10.1029/2002JB002166.

Chiaraluce, L., Amato, A., Cocco, M., Chiarabba, C., Selvaggi, G., Di Bona, M., Piccinini, D., Deschamps, L., Margheriti, F., Courboulex, F., Ripepe, M., 2004. Complex normal faulting in the Apennines thrust-and-fold belt: the 1997 seismic sequence in central Italy. Bulletin of the Seismological Society of America 94, 99–116.

Chiaraluce, L., Barchi, M., Collettini, C., Mirabella, F., Pucci, S., 2005. Connecting seismically active normal faults with Quaternary geological structures in a complex extensional environment: the Colfiorito 1997 case history (northern Apennines, Italy). Tectonics 24, TC1002. doi:10.1029/2004TC001627.

Collettini, C., Chiaraluce, L., Pucci, S., Barchi, M.R., Cocco, M., 2005. Looking at fault reactivation matching structural geology and seismological data. Journal of Structural Geology 27, 937–942. doi:10.1016/j.jsg.2004.10.016.

Dela Pierre, F., Ghisetti, F., Lanza, R., Vezzani, L., 1992. Palaeomagnetic and structural evidence of Neogene tectonic rotation of the Gran Sasso range (central Apennines, Italy). Tectonophysics 215, 335–348.

Dewey, J.F., Helman, M.L., Turco, E., Hutton, D.H.W., Knott, S.D., 1989. Kinematics of the western Mediterranean. In: Coward, M.P., Dietrich, D., Park, R.G. (Eds.), Alpine Tectonics. Geological Society Special Publications, London, pp. 265–283.

Ekström, G., Morelli, A., Boschi, E., Dziewonski, A.M., 1998. Moment tensor analysis of the central Italy earthquake sequence of September–October 1997. Geophysical Research Letters 25, 1971–1974.

Elter, P., Giglia, G., Tongiorgi, M., Trevisan, L., 1975. Tensional and compressional areas in recent (Tortonian to Present) evolution of north Apennines. Bollettino di Geofisica Teorica ed Applicata 17, 3–18.

Huc, M., Main, I.G., 2003. Anomalous stress diffusion in earthquake triggering: correlation length, time dependence, and directionality. Journal of Geophysical Research 108 (B7), 2324. doi:10.1029/201JB001645.

Kagan, Y.Y., 1990. Random stress and earthquake statistics: spatial dependence. Geophysical Journal International 102, 573–583.

Kagan, Y.Y., 1991. 3-D rotation of double-couple earthquake sources. Geophysical Journal International 106, 709–716.

Kagan, Y.Y., 1992a. On the geometry of an earthquake fault system. Physics of the Earth and Planetary Interiors 71, 15–35.

Kagan, Y.Y., 1992b. Correlations of earthquake focal mechanisms. Geophysical Journal International 110, 305–320.

Kagan, Y.Y., Knopoff, L., 1985a. The first-order statistical moment of the seismic moment tensor. Geophysical Journal of the Royal Astronomical Society 81, 429–444.

Kagan, Y.Y., Knopoff, L., 1985b. The two-point correlation function of the seismic moment tensor. Geophysical Journal of the Royal Astronomical Society 83, 637–656.

Kaverina, A.N., Lander, A.V., Prozorov, A.G., 1996. Global creepex distribution and its relation to earthquake-source geometry and tectonic origin. Geophysical Journal International 125, 249–265.

Knox-Robinson, C.M., Gardoll, S.J., 1998. GIS-stereoplot: an interactive stereonet plotting module for ArcView 3.0 geographic information system. Computers & Geosciences 24, 243–250.

Koopman, A., 1983. Detachment Tectonics in the central Apennines, Italy. Geologica Ultraiectina 30, 1–155.

Lavecchia, G., 1985. Il sovrascorrimento dei Monti Sibillini: analisi cinematica e strutturale. Bollettino della Societa Geologica Italiana 104, 161–194.

Lavecchia, G., Brozzetti, F., Barchi, M., Menichetti, M., Keller, J.V.A., 1994. Seismotectonic zoning in east-central Italy deduced from an analysis of the Neogene to present deformations and related stress fields. Geological Society of America Bulletin 106, 1107–1120.

Marrett, R., Allmendinger, R.W., 1990. Kinematic analysis of fault-slip-data. Journal of Structural Geology 12, 973–986.

Michael, A., 1984. Determination of stress from slip data: faults and folds. Journal of Geophysical Research 89, 11517–11526.

Morelli, A., Ekström, G., Olivieri, M., 2000. Source properties of the 1997–98 central Italy earthquake sequence from inversion of long-period and broad-band seismograms. Journal of Seismology 4, 365–375.

Morris, A., Ferrill, D.A., Henderson, D.B., 1996. Slip-tendency analysis and fault reactivation. Geology 24, 275–278.

Nemcok, M., Lisle, R.J., 1995. A stress inversion procedure for polyphase fault/slip data sets. Journal of Structural Geology 17, 1445–1453.

Nemcok, M., Kovác, D., Lisle, R.J., 1999. A stress inversion procedure for polyphase calcite twin and fault/slip data sets. Journal of Structural Geology 21, 597–611.

Nieto-Samaniego, A.F., Alaniz-Alvarez, S.A., 1997. Origin and tectonic interpretation of multiple fault patterns. Tectonophysics 270, 197–206.

Nostro, C., Chiaraluce, L., Cocco, M., Baumont, D., Scotti, O., 2005. Coulomb stress changes caused by repeated normal faulting earthquakes during the 1997 Umbria–Marche (central Italy) seismic sequence. Journal of Geophysical Research 110, B05S20. doi:10.1029/2004JB003386.

Orife, T., Lisle, R.J., 2003. Numerical processing of palaeostress results. Journal of Structural Geology 25, 949–957. doi:10.1016/S0191-8141(02)00120-7.

Ramsay, J.G., Huber, M.I., 1987. The techniques of modern structural geology. Folds and Fractures, vol. 2. Academic Press, London.

Scisciani, V., Tavarnelli, E., Calamita, F., 2002. The interaction of extensional and contractional deformations in the outer zones of the central Apennines, Italy. Journal of Structural Geology 24, 1647–1658. doi:10.1016/S0191-8141(01)00164-X.